Identifying Land Subsidence Using Global Digital Elevation Models

Kazimierz Becek, *Senior Member, IEEE*, Khairunnisa Ibrahim, Caglar Bayik, Saygin Abdikan, Hakan S. Kutoglu, Dariusz Glabicki, and Jan Blachowski

***Abstract*—Recent developments in space-based surveying methods of the Earth's topography, including the differential interferometric synthetic aperture radar (DInSAR), have increased the availability of options for monitoring land subsidence. However, DInSAR methods require expert knowledge and specialized software, and they are time-consuming. Here, we demonstrate that a land subsidence signal can be identified in the differences in the freely available global digital elevation models (e.g., SRTM and TanDEM-X) using a simple statistical method. This finding opens up a venue to develop a computer application to identify land subsidence or uplift of a few decimeters per at least a decade order. Such an application enables monitoring the effects of underground mining, seismic/tectonic movements, landslides, volcanic activities, and similar effects on the Earth's topography. It can also provide a valuable and cost-effective tool for studying land deformation.**

***Index Terms*—Digital elevation models (DEMs), geodesy, geophysical measurement techniques, geospatial analysis, level measurement, synthetic aperture radar, terrain mapping.**

I. Introduction

UNDERGROUND mining has contributed to several undesirable physical effects on the Earth's surface, including mining-induced land deformations and landslides. In populated areas, underground mining can interfere with the anthropogenic infrastructure, leading to extensive damage or destruction and endanger human safety. Some measures have been proposed to mitigate the effects of mining. Nevertheless, the successful implementation of these measures depends on several factors, including financial constraints, local politics, and precise and updated information on the spatial extent and velocity of land deformation. The latter can be obtained because of recent developments in the spaceborne surveying methods of the Earth's surface, including the interferometric synthetic aperture radar (InSAR) [1], [2], differential interferometric synthetic aperture radar (DInSAR) [3], persistent scatterer InSAR [4], [5], and small baseline subset (SBAS) InSAR method [6], which have significantly enriched the arsenal of surveying methods for monitoring and investigating land deformation. However, SAR interferometry-based methods require extensive computing resources and are time-consuming. Moreover, these approaches demonstrate some technical incompetence under certain circumstances when detecting surface deformations. Therefore, alternatives are needed that are simpler in approach, more efficient, and more accurate but are also cost-effective in terms of the time required to process data.

This article demonstrates that freely available global digital elevation models (DEMs) can identify land subsidence/uplift caused by mining activities or other processes. Our approach involves comparing DEMSs that were captured at two distant time points during which the deformation occurred. Although this method is straightforward, it has deterred other researchers from developing it further because of the limitations of the vertical accuracy of global DEMs in the order of a few meters and the magnitude of land deformations at the level of submeters, sometimes larger. Nevertheless, we have managed to develop this approach by performing the following tasks to reach the aim of this project.

1) We developed a raster of mining-induced land deformation of a test area in Turkey using the SBAS InSAR [6] method and used it to split the area of interests (AOI) in the deformation and no-deformation regions.
2) We calculated the difference between the recent (2014) TanDEM-X DEM and the 2000 Shuttle Radar Topography Mission (SRTM) elevation data product for the deformation and no-deformation areas. Our calculations detected a signal in the differences between the DEMs, which correlates with the land deformations.

This finding provides an impetus for developing an application that can quickly and efficiently scan and calculate the differences in the existing global DEMs and identify land deformations of both anthropogenic and natural origins that have occurred during the first decade of the third millennia around the world.

The rest of this article is organized as follows. Section I provides the background of the study. Section II introduces the area of interest. Section III presents the specifications of the dataset used in this article. Section IV provides the proposed

Manuscript received February 26, 2021; revised June 28, 2021; accepted August 30, 2021. Date of publication September 8, 2021; date of current version September 20, 2021. The work of Kazimierz Becek was supported by the Polish National Agency for Academic Exchange. (*Corresponding author: Kazimierz Becek.*)

Kazimierz Becek, Dariusz Glabicki, and Jan Blachowski are with the Geoengineering, Mining and Geology Department, Wroclaw University of Science and Technology, 50-370 Wroclaw, Poland (e-mail: kazimierz.becek@pwr.edu.pl; dariusz.glabicki@pwr.edu.pl; jan.blachowski@pwr.edu.pl).

Khairunnisa Ibrahim is with the University of Brunei Darussalam, BE1410 Gadong, Brunei (e-mail: charismanisa@gmail.com).

Caglar Bayik and Hakan S. Kutoglu are with the Geomatics Engineering Department, Zonguldak Bulent Ecevit University, Zonguldak 67100, Turkey (e-mail: caglarbayik@beun.edu.tr; shakan.kutoglu@beun.edu.tr).

Saygin Abdikan is with the Geomatics Engineering Department, Hacettepe University, Ankara 06800, Turkey (e-mail: sayginabdikan@hacettepe.edu.tr).

Digital Object Identifier 10.1109/JSTARS.2021.3110438

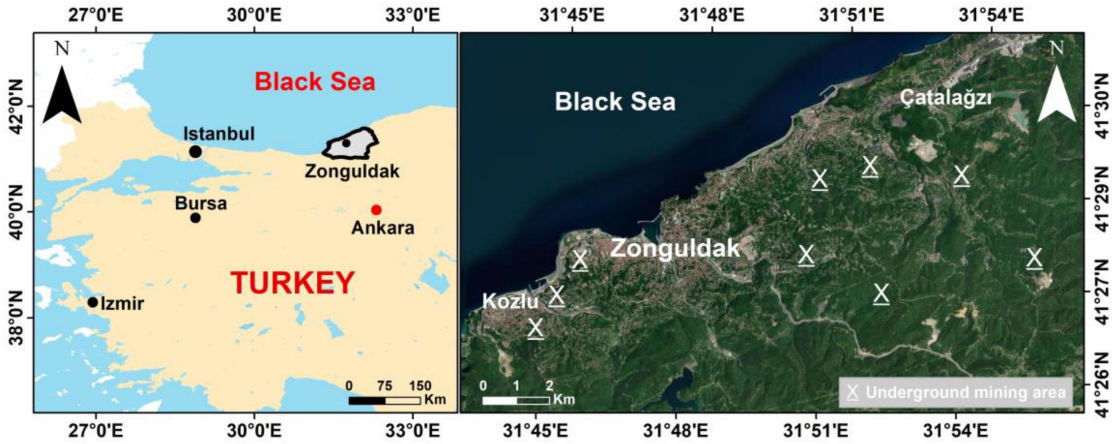

Fig. 1. Geographic context of the AOI.

method. Section V presents the visualization and the quantitative interpretation of the results, including a brief discussion of the results. Finally, Section VI concludes this article.

II. Area of Interests

The AOI is situated in the central northern part of Turkey. It borders the Black Sea to the north and covers 17. km × 11.5 km (W-E/N-S). The geographic coordinates of the SW/NE corners of the AOI are (WGS84): (Lat/Lon): 41° 24'44"/31° 43'24" and 41° 31'4"/31° 56'5". Fig. 1 shows the geographic settings of the AOI.

The topography of the AOI is characterized by moderate relief. The average terrain elevation is approximately 233 m a.m.s.l. The lowest and highest points are at sea level and 600 m a.m.s.l., respectively. The dominant land cover (approximately 75%) is forest, 90% of deciduous tree species. The coastal strip comprises human settlements, including transportation and industrial infrastructure. The largest settlements are Zonguldak and Kozlu, with a total population of approximately 1 50 000 residents combined, and they are located in the western section of the AOI. The largest industrial facility is a large power plant at Çatalağzı, and it is located in the central north of the AOI. The main industry is the underground mining of hard coal. The mining area is located in the Zonguldak and Kozlu towns and the AOI's central part. Mining has been conducted in the area for over 100 years [7]. Mining operations have been carried out at a depth of 400–600 m. Over the years, many land deformation and landslide events have been observed, leading to severe damage to properties and even deaths [7].

III. Data

A. SRTM Digital Elevation Data Product

The SRTM-1" (v.3) (SRTM) elevation data product is a well-known global DEM that has been used for many types of geospatial studies in several branches of science [8]. In February 2000, the space shuttle "Endeavour" hosted the unique single-pass SAR instrument to acquire the data for processing using the InSAR method to generate a semiglobal DEM. The SRTM heights represent the phase center of vegetated areas located below the canopy and above the terrain. This effect is sometimes described as vegetation bias. The SRTM data product is available at one and three arcsec resolutions (approximately 30 m or 90 m at the equator). The three arcsec version was produced by the averaging of the original one arcsec model. The vertical accuracy of SRTM is approximately 2 m (one sigma for horizontal surfaces—see METHODS/B section for more details), which is well over the mission's requirement [9]–[12]. Version 3 of the SRTM-1" was used as a reference dataset in this article. The horizontal reference system used was WGS84, and elevation was provided with reference to the Earth gravity model (EGM96). As the data for the SRTM product were captured during winter in the northern hemisphere, the deciduous forests were in the leaves-off state, allowing for partial penetration of vegetation by the C-band microwaves ($\lambda = 5.3$ cm or $f = 5.7$ GHz) of the SRTM mission SAR system [13].

B. TanDEM-X Digital Elevation Data Product

TanDEM-X 30 m DEM (TDX) is an elevation data product developed from the data captured by the TerraSAR-X/TanDEM-X mission using the X-band ($\lambda = 3.1$ cm or $f = 9.7$ GHz) SAR instrument [14]. The TDX is a quasi-digital surface model (DSM), i.e., the elevations represent the phase center located between the canopy and the terrain in vegetated areas [13]. The spatial resolution of the TDX models is one arcsec or approximately 30 m at the equator. One of the authors of this article developed this model using bilinear resampling of 0.4 arcsec (approximately 12 m at the equator) resolution data provided by the German Aerospace Center (Deutsches Zentrum für Luft- und Raumfahrt - DLR) as part of a research project. However, the TanDEM-X DEM can be downloaded at a three-arcsec (approximately 90 m at the equator) resolution from https://geoservice.dlr.de/web/dataguide/tdm90/ free of charge. The 0.4 arcsec DEM is available as a commercial product known as WorldDEM^{TM} [15]. The vertical accuracy of the TDX is approximately 2 m (one sigma for horizontal surfaces—see

METHODS/B section for more details), and the accuracy of the WorldDEM™ is approximately 0.8 m (one sigma) [15]. As the data source for the TDX and WorldDEM™ is the same, this study's conclusions can be expected to be valid for both models. The horizontal reference system for TDX is WGS84. The vertical datum is the WGS84 ellipsoid. According to the metadata, the SAR data were acquired during the satellites' 27 passes between February 17, 2011 and August 27, 2014, and then averaged. Fifteen images were taken during the leaves-off state of vegetation (autumn to early spring). This means that a vegetation bias is present in the TDX. Note that the magnitude of the vegetation bias varies with the microwave band [13]. In our case, the SRTM and TDX were created using the C-band and X-band, respectively. Furthermore, we omitted the different magnitudes of the vegetation bias of SRTM and TDX from the analysis.

C. SAR Data

We used the SAR data captured by the Copernicus Sentinel-1A/B satellite mission [16]. A total of 103 images acquired in the Interferometric Wide-Swath mode from the descending orbit (orbit no. 65) were used in the study. The images were acquired between January 2018 and October 2019.

D. Reference DEM

Many studies on the SRTM and TDX models' vertical accuracy have identified a vertical bias (e.g., [12]). To identify and offset the bias, we used a higher accuracy and a recent DEM model called HQM. HQM is a DSM produced from stereo pairs of 2017 aerial photography. The original DSM was produced at a resolution of 0.45 m, but it was available to the authors at a 5 m resolution. The vertical accuracy is 1.52 m (one sigma) [17]. The HQM is referenced to the national height system of Turkey (orthometric system). HQM was further downsampled using the bilinear method to a one arcsec resolution in the investigated DEMs. The model's vertical accuracy assessment was confirmed using the runway method [12], which was carried out at a few selected flat sites, including sports fields and highways.

IV. Methods

A. SBAS Method

The SBAS method is a version of the DInSAR method (e.g., [18]). It was developed to monitor land deformation as a function of time [6]. This method allows for estimating the deformation's velocity with an accuracy of approximately 5 mm/yr [18]–[20]. Many studies have described the SBAS data processing procedure (e.g., [2], [5], and [21]), and its applications include assessing land subsidence under large cities [22], [23], monitoring land subsidence caused by groundwater level change [24], monitoring volcano eruption [25], and assessing mining-induced land deformation [26]. One of the initial SBAS processing steps is to form interferograms based on pairs of images taken from different orbit (spatial baseline). The second condition for selecting images for the interferograms is to restrict the temporal baseline (time between two image acquisitions). We constrained the SBAS calculations by a temporal baseline of fewer than 36 days and a spatial baseline of less than 100 m. Given these conditions, 326 interferograms were formed from the data captured by the Sentinel-1 satellites. The SRTM-1" DEM was used to subtract the topographic phase from the interferograms, a step in the SBAS data processing. As a final result, the raster of the line-of-sight (LOS) deformation was obtained. The LOS deformation is a composite vector of land subsidence and horizontal displacement. As we processed the descending orbit images only, splitting the LOS vector into the north/east components was impossible. The resulting raster had a spatial resolution of approximately 4 arcsec (approximately 120 m). The reduced resolution of the raster was constrained by the computation assets available for this project. The interferometric calculation and SBAS processing were performed in the GMTSAR software [27]. The SNAPHU software was used to unwrap the interferograms [28].

B. Vertical Accuracy Model of the DEMs Difference

The vertical error of a pixel in a DEM can be modeled as a sum of the following three statistically independent error components: the instrument-induced (*I*), target-induced (*T*), and environment-induced (*E*) component. This can be written as follows [11]:

$$\sigma_{DEM}^2 = \sigma_I^2 + \sigma_E^2 + \sigma_T^2 \tag{1}$$

where $\sigma_I^2,\ \sigma_E^2,$ and σ_T^2 are the variance of the *I*, *E,* and *T* error components.

The *T* error component can be calculated for a pixel from [11]

$$\sigma_T^2 = \frac{1}{12}\, d^2 tan^2\,(s) \tag{2}$$

where σ_T^2 is the variance of the *T* error, *d* is pixel size, and *s* is the slope at a given pixel.

The *T* error component equals 0 for horizontal or flat pixels (slope $s = 0$). For nonhorizontal pixels ($s > 0$), the magnitude of the *T* error depends on both the pixel size *d* and the slope *s*.

The *I* error component is caused by the instrument, method, and processing of the data used to calculate pixel height. The *I* error was estimated in [11] and [12] for SRTM, and for WorldDEM™ (TanDEM-X) in [15]. The *I* error for SRTM and TanDEM-X are provided in the DATA section (parts A and B) as 2 m (one sigma).

The *E* error is caused by the atmosphere's chaotic properties and the dielectric properties of the Earth's surface. The magnitude of the error is approximately tenfold smaller than the *I* or *T* errors. Hence, we omit the *E* error. The vertical accuracy can be expressed as the average of the $I + T$ error of all pixels in the DEM. In this study, we used the difference between the two DEMs. The error of the difference is given by

$$\sigma_{diff}^2 = \sigma_{DEM1}^2 + \sigma_{DEM2}^2 \tag{3}$$

where σ_{DEM1}^2 and σ_{DEM2}^2 are the variance of the error of DEM_1 and DEM_2, respectively.

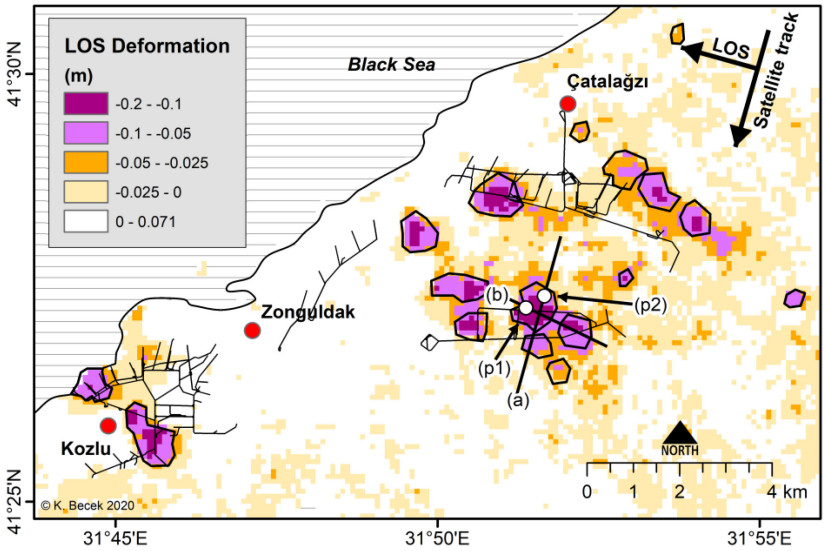

Fig. 2. LOS deformation map from the SBAS processing of the Sentinel-1A/B SAR data. The deformations occurred between January 2018 and October 2019. Location of the major underground mining tracks are marked with a black line. The satellite track and the look vector are indicated on the map. Symbols (a) and (b) are placed at the beginning of the profile lines shown in Fig. 2. Symbols (p1) and (p2) indicate the points on the profile lines for which the LOS deformation time series are constructed. They are also shown in Fig. 3.

V. Results

A. LOS Deformation

Fig. 2 shows a map of the LOS deformations calculated for January 2018 and October 2019 based on the Sentinel-1 data. The deformation areas are manually outlined (solid black line) in Fig. 2 and are denoted as the "deformation" and "no-deformation" areas. Deformations appear to be closely associated with underground mining, excavation, or stockpiling operations on the surface. The AOI may also be affected by tectonic uplift of up to 0.006 m/yr [29].

Fig. 3 shows the LOS deformation's time series for two profiles marked as (a) and (b) in Fig. 2. Each profile has 103 lines. The LOS deformation lines exhibit a "complicated" spatially explicit shape, suggesting an anisotropic character of the underlying deformation forces and geomorphological/geological constraints.

We also investigated LOS deformation as a function of time. Fig. 4 shows the LOS deformation profiles for two randomly selected points (p1) and (p2) on the profile lines (a) and (b). The LOS deformation for both points appears to progress at a steady rate.

Fig. 5 shows the histograms of the LOS deformations for the deformation (a) and no-deformation areas (b). The histograms are bimodal (negative skew), suggesting that two processes contribute to deformation. The histograms were modeled using the generalized Gaussian pdf. Gauss 1 and Gauss 3 curves represent vegetation-free areas' deformation, whereas Gauss 2 and Gauss 4 represent vegetation areas. The limited penetrability of the C-band of vegetation is responsible for the high standard deviation of Gauss 2 and Gauss 4 pdfs. The standard deviation of the Gauss 3 pdf (no-deformation) of approximately 4 mm is consistent with the results found in previous studies [18]–[20].

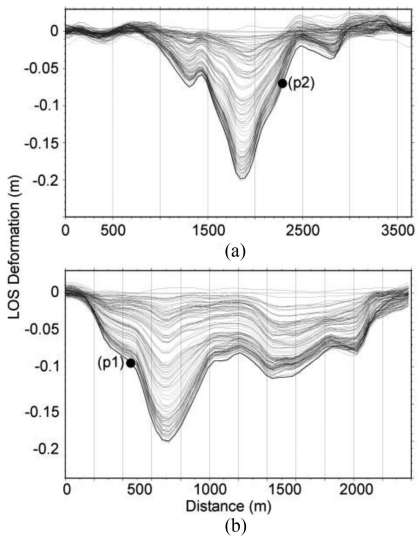

Fig. 3. LOS deformation progression for profiles (a) and (b) marked in Fig. 1. The position of symbols (a) and (b) in Fig. 1. coincides with the starting points of the profiles. There are 103 lines in the plot. The deformation magnitude/rate depends on the location on the profile. Points (p1) and (p2) are discussed further in this article.

The mean LOS deformation in the deformation area (both Gauss 1 and Gauss 2 considered) is approximately −0.052 m, and it occurred from January 2018 to October 2019. This value corresponds to a mean deformation rate of approximately −0.003 m/month.

B. DEM Difference

The difference in TDX *minus* SRTM is used as a data source to identify the subsidence regions. In the following sections, we analyze the properties of the DEM difference.

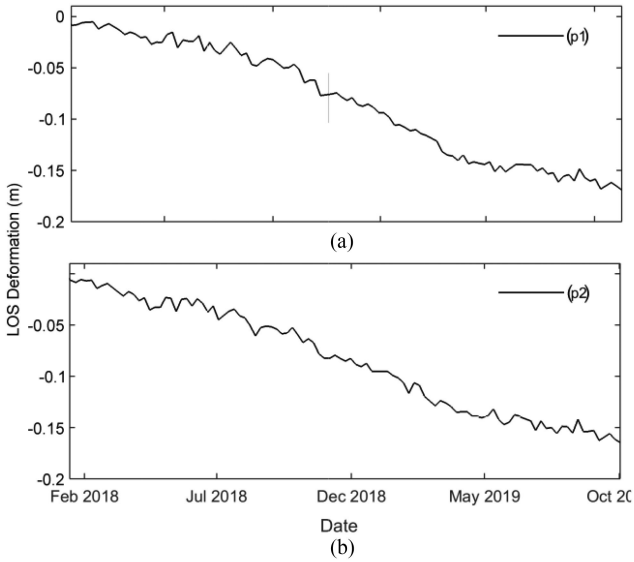

Fig. 4. LOS deformation time series for two points marked as (p1) and (p2) in Fig. 1 and in Fig.2. The rate of the deformations appears to follow a linear trend.

The TDX and SRTM models usually exhibit an elevation bias with respect to the local orthometric vertical reference systems. This bias is one of the components of a standard vertical accuracy statement referred to as the root mean square error (RMSE). Equation (4) outlines a well-known relationship between the RMSE and the bias

$$RMSE^2 = (E[x])^2 + \sigma^2 \tag{4}$$

where $RMSE^2$ is the variance, $E[x]$ is the average of x or the bias, σ is the standard deviation of x, and x is a vector of differences between the reference and the actual pixels of DEM.

The source of this bias may be related to the calibration of the SAR instruments, the precision of the EGM96 geoid model, and the local height system's characteristics. Depending on the world's region, the bias may be negative or positive and is in the order of 1 m [12]. In our case, we estimated the bias by comparing the average heights of several flat objects (sports fields) in the AOI calculated from the HQM, SRTM, and TDX. We corrected the DEMs by subtracting the bias from the DEMs. We found that the bias for the TDX (including the geoid undulation) was 32.38 m (TDX was too high); the SRTM bias was -1.52 m (SRTM was too low). As the bias was estimated on leaves-free and stable terrain features, bias correction should not affect the magnitude of subsidence. Fig. 6 shows a map of the differences between the corrected TDX and SRTM. The map does not show any subsidence correlated with the LOS deformation areas identified by the map's black outline. This is due to some isolated outliers and large-scale vertical terrain changes caused by excavation works and stockpiling operations. To investigate the structure of the difference in TDX *minus* SRTM, we analyzed its histogram.

The histograms of the difference between the corrected TDX *minus* SRTM models are shown in Fig. 7. We performed the one-sample Kolmogorov–Smirnov test to verify the hypothesis

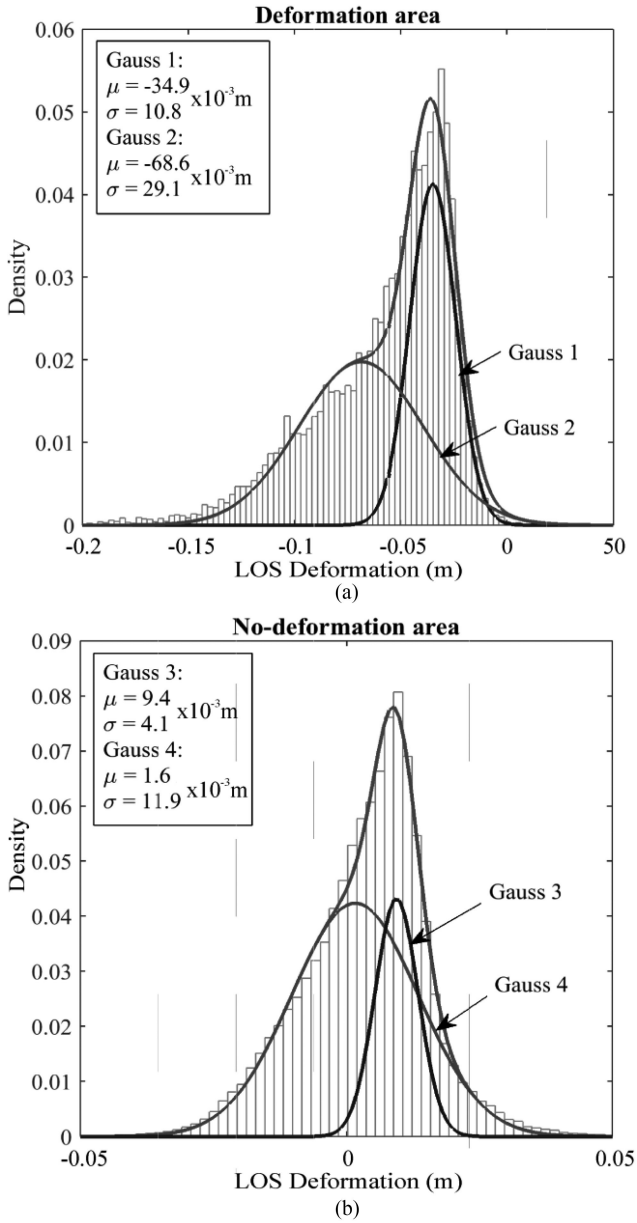

Fig. 5. Histograms of the average LOS deformation (as observed from January 2018 to October 2019) in (a) deformation area and (b) no-deformation area. Histograms are modeled using a two-term generalized Gaussian pdf. The mean and standard deviation are also shown.

that the differences follow a normal distribution. The result suggests that the differences do not follow a normal distribution at the 5% significance level. This finding contradicts some authors' attempts who "forcefully" model the histogram using the normal pdf without conducting a proper statistical test. Instead of applying a similar approach, we used the Laplace pdf to model the histogram because terrain elevations follow exponential pdf. Hence, the Laplace pdf much better models the histogram of differences between two terrain surfaces.

Equation (5) shows the Laplace pdf of a random variable x

$$f\ (x\mu, b) = \frac{1}{2}\, b * \exp\left(-\frac{|x-\mu|}{b}\right). \tag{5}$$

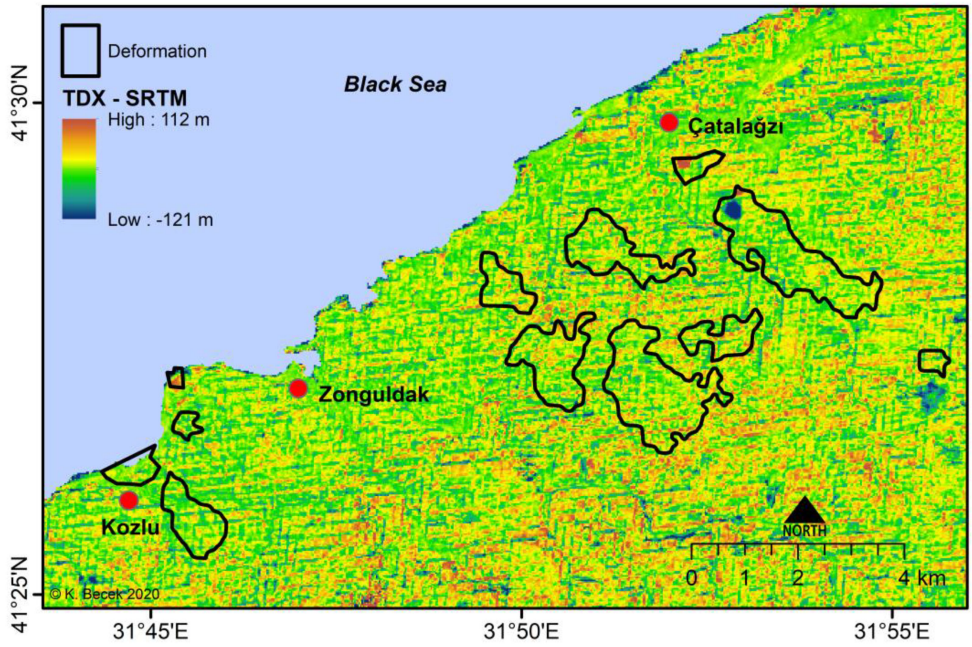

Fig. 6. Map of the difference in TDX *minus* SRTM. The difference was calculated after removing the bias from TDX and SRTM. The map does not reveal the subsidence signal simply because of the much larger vertical range of the difference versus the mining-induced subsidence. Even the SBAS-estimated location of the deformation areas (black outlines) does not identify any subsidence signal. Several large subsidence/uplift areas were caused by excavation or stockpiling operations.

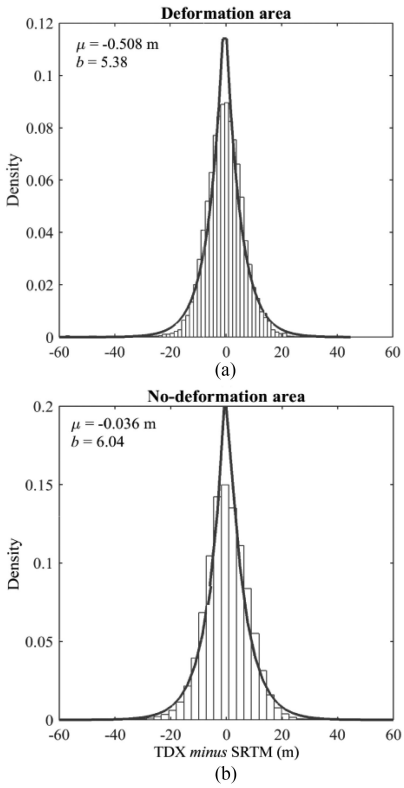

Fig. 7. Histograms of the differences between TDX *minus* SRTM for (a) deformation and (b) no-deformation areas. The Laplace pdf curves, including the location parameter μ and scale parameter b, are also shown. The location parameter corresponds to the average value of a random variable in the case of a normal distribution. The scale parameter allows for calculating the standard deviation according to (7).

The maximum likelihood estimator of μ is the sample median, equivalent to the average value of a random variable in the case of a normal pdf. The estimator of b is the mean absolute deviation from the location parameter μ, and it is expressed by [30]

$$b = \frac{1}{n} \sum_{i=1}^{i=N} |x_i - \mu| \tag{6}$$

where i is the number of pixels ($\sim$186000).

The variance of the DEM difference can be calculated from

$$\sigma^2 = 2b^2. \tag{7}$$

The average value of μ and σ was then used in the following considerations instead of the calculated estimates assuming a normal pdf.

The calculations yielded the location parameter $\mu = -0.51$ m. ($\sigma = 7.61$ m) and -0.04 m ($\sigma = 8.54$ m) for the deformation and no-deformation area, respectively.

The average difference μ in the deformation area is smaller than that in the no-deformation area by -0.47 m ($= -0.51$ m $+$ 0.04 m), suggesting the difference in TDX *minus* SRTM contains a deformation signal. To verify whether this observation is statistically significant, we conducted a hypothesis test. The null hypothesis is as follows (H_0): The average difference in TDX *minus* SRTM $\mu = 0$ m. The alternative hypothesis is as follows H_A: The average difference $\mu < 0$ m. To perform the test, we randomly selected 1000 pixels in the deformation areas. The mean difference for these random points was -0.5 m ($s =$ 7.8 m). We found a p-value $= 0.025 < 0.05$ or a confidence level of 95%. These results enabled us to reject the null hypothesis at the 95% confidence level. This result indicates that the difference

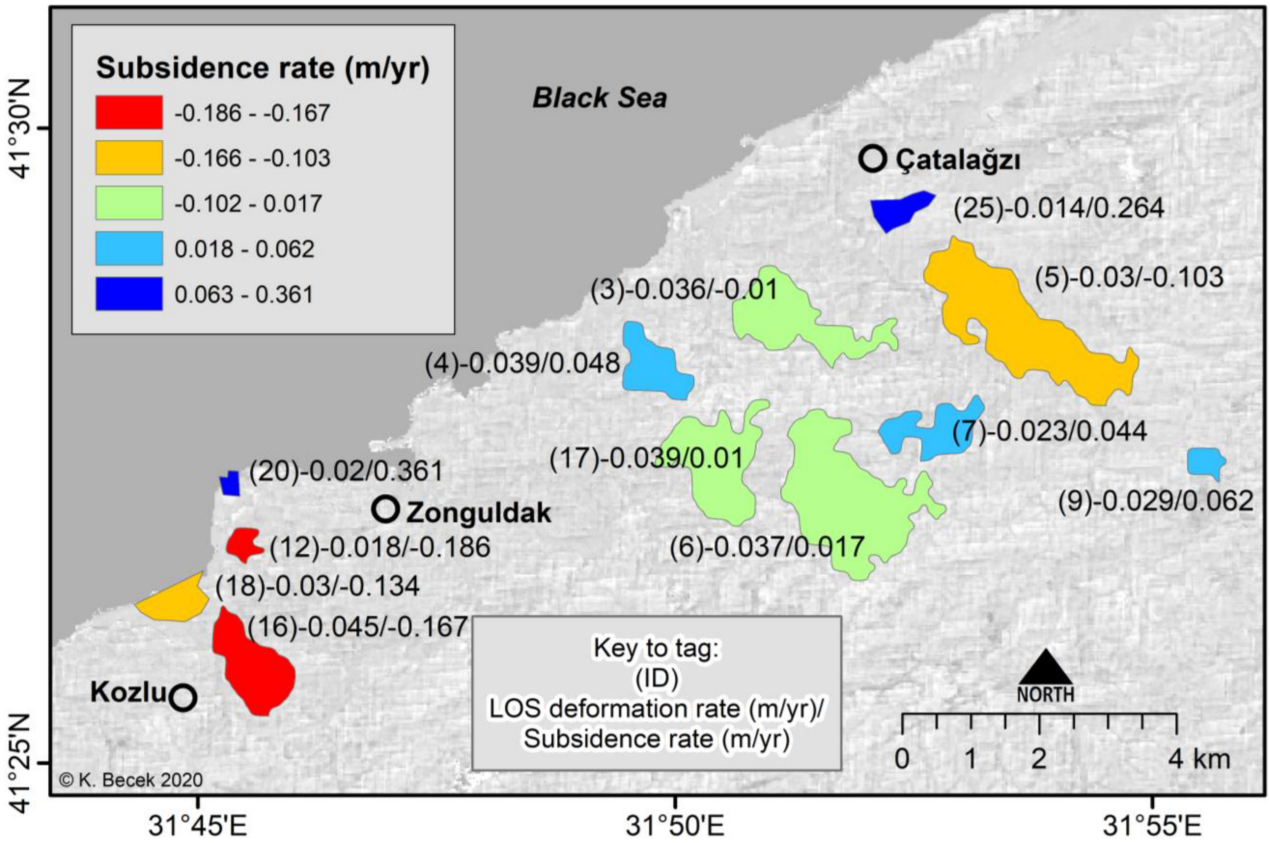

Fig. 8. TDX *minus* SRTM subsidence and LOS deformation annual rates in deformation regions. The regions are annotated by the "(ID) LOS deformation rate (m/yr)/TDX *minus* SRTM subsidence rate (m/yr)" tags.

in TDX *minus* SRTM in the deformation and no-deformation areas is statistically significant.

C. Spatial Variability of the DEM Difference (Subsidence)

Changes in topography may be caused by several phenomena, including underground mining, excavation works, stockpiling of various materials, and seismic/tectonic movements. These surface changes can vary in magnitude, duration, and when they commenced/concluded. These modifications may also be caused by more than one phenomenon, for example, subsidence combined with stockpiling operations. Therefore, a reference time frame is needed to study the spatio-temporal topography changes. In our case, the reference frame is approximately 14 years (between 2000 and 2014). Fig. 8 shows a map of deformation regions annotated with the mean LOS deformation (m)/mean subsidence (m) (TDX *minus* SRTM). For example, (3)-0.061/−0.14 means that the region ID = 3 exhibits a LOS deformation of −0.036 m/yr and the subsidence rate (TDX *minus* SRTM) of −0.01 m/yr. Fig. 8 reveals differences between deformation regions in terms of the mean subsidence within the region. The red regions (IDs 12 and 16) exhibit the most considerable subsidence rate. However, it also could be due to some excavation operations. Regions ID = 20 and 25 show an uplift signal caused by stockpiling operations. Table I provides a possible interpretation of the spatio-temporal variation of the subsidence/deformation of deformation regions.

TABLE I
INTERPRETATION OF THE SPATIO-TEMPORAL VARIATION OF THE SUBSIDENCE/DEFORMATION OF DEFORMATION REGIONS

ID	LOS deformation rate[a] (2018 –2019) (m/yr)	TDX-SRTM Subsidence rate[b] (2000-2014) (m/yr)	Interpretation
3	-0.036	-0.011	S
4	-0.039	0.048	S + St
5	-0.030	-0.103	S + E
6	-0.037	0.017	Recent D/ No S
7	-0.023	0.044	S + St
9	-0.029	0.062	S + St
12	-0.030	-2.61	S + E
16	-0.075	-2.34	S + E
17	-0.065	0.15	Recent D/ No S
18	-0.050	-1.88	S + E
20	-0.033	5.05	S + St
25	-0.023	3.69	S + St

[a]Sentinel-1A/B estimates
[b]TDX *minus* SRTM
D – Deformation; S – Subsidence; Stp – Stockpiling; E – Excavation.

D. Subsidence Versus LOS Deformation

As demonstrated in the previous section, the TDX *minus* SRTM difference contains a signal linked to land deformation. One may be interested in a quantitative relationship between the

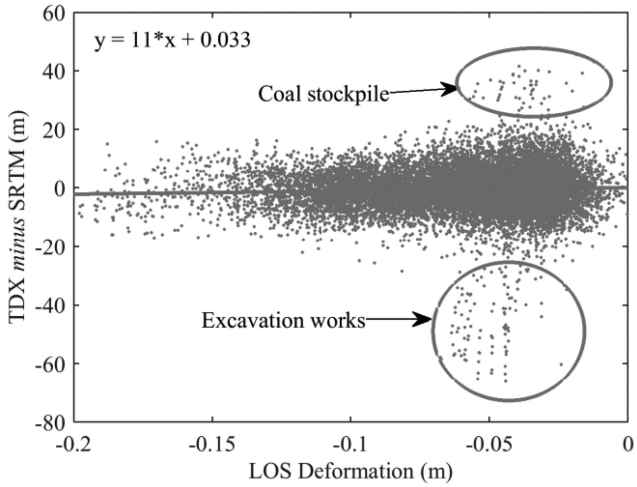

Fig. 9. TDX *minus* SRTM versus LOS deformation, including a regression line, and a regression equation. Correlation coefficient = 0.046, p-value = $2.5274 \times 10^{-9} < 0.01$ (Pearson's test). The ellipses (circled) identify the pixels representing the topography changes due to excavation or stockpiling operations.

TDX *minus* SRTM difference and the LOS deformations. It is not hard to imagine that such a relationship would be relatively weak as a few factors disturb such a relationship. These factors include low resolution of the LOS deformation raster (4") versus the DEM resolution (1"), short (approx. 20 months) time series of LOS deformations, natural changes in vegetation cover due to phenology, and re-/de-forestation might occur. Hence, such a relationship's practical value can have limited applicability, perhaps as a raw estimate only. Nevertheless, in the following, we present an attempt to estimate the LOS deformation as a function of the TDX minus SRTM Fig. 9 shows a scattergram of the TDX *minus* SRTM difference versus LOS deformation. Pearson's correlation test yielded a correlation coefficient of 0.046 with a p-value of $2.5274 \times 10^{-9} < 0.01$. As expected, this result confirms that a linear relationship between the LOS deformation and TDX *minus* SRTM is indeed a weak one due to a high level of noise of various origins.

The ellipses in Fig. 9 delineate the outliers, which were considered in the hypothesis tests. A detailed inspection of the outliers showed that they were not related to the subsidence but rather to the open pit excavations (at 31°52'52" E, 41°29'03" N) and stockpiling (at 31°52'09" E, 41°29'28" N) of coal and byproducts of the power plant in Çatalağzı. These operations can be recognized on satellite images using the Google Earth service. They are also present in Fig. 8 within the region ID = 5 and 25.

Note that the LOS deformations occurred within 20 months (between January 2018 and October 2019). Assuming that the detected deformations are only the latest in a long-running series of land changes in the AOI since mining began (approximately 100 years ago) or even longer, this analysis shows a single snapshot of the process.

VI. Conclusion

This study is the first to use the global DEMs to identify land subsidence in the order of a few decimeters per at least a decade to the authors' knowledge. It is a straightforward approach with an essential requirement of a sufficient period between selected DEMs' capture. This approach can be applied to identify vertical land deformation, including tectonic-, seismic-, landslide-, and volcanic-induced. In this study, the SBAS estimated subsidence's velocity was −0.041 m/yr, which is consistent with the TDX *minus* SRTM estimated subsidence velocity of −0.034 m/yr.

The sensitivity of the proposed method for detecting vertical land deformations is a function of the accuracy characteristics of the input DEMs, the land cover, and the roughness of the terrain. It is reasonable to anticipate that over time, the accuracy of global DEMs will gradually increase, paving the way for identifying slower land deformation processes with higher accuracy. However, the impact of land cover on the accuracy of the InSAR/photogrammetry-based DEMs cannot be overcome. In addition, the impact of the topography can be limited by improving the ground resolution of the DEMs. Another limitation of the proposed method is that it records a cumulative vertical land deformation.

We also tested the AW3D30 m [31]/SRTM pair of DEMs. Again, results (not shown here) were similar, suggesting that other DEMs could be used for similar studies on land subsidence anywhere in the world. An attractive research project would be to compare a DEM derived from contours [32] with SRTM or any other global DEM.

To conclude, this study proves this method's potential to detect vertical land deformations using readily available DEMs. Developing a dedicated software that implements this technique will save time and cost to calculate the subsidence raster for a given AOI.

Appendix

Data used in this project are available in [33].

Acknowledgments

The authors would like to thank Dr. Tom G. Farr of Jet Propulsion Laboratory for his meaningful remarks that significantly improved the manuscript's early version and as well as Prof. Chris Rizos of UNSW, Sydney, Australia, and Prof. Shuanggen Jin of the Shanghai Astronomical Observatory, Chinese Academy of Sciences, Beijing, China, for their valuable comments. The author Kazimierz Becek would like to thank the German Aerospace Center (DLR) for the TandDEM-X data obtained as a part of the DEM_GEOL1272 research project, and acknowledges support and feedback received during his participation in the 9th International Scientific-Technical Conference, Sept. 2019, Lublin, Poland from National Agency for Academic Exchange (NAWA).

References

[1] M. Crosetto and P. Pasquali, "DSM generation and deformation measurement from SAR data," in *Advances in Photogrammetry, Remote Sensing and Spatial Information Sciences*, Z. Li, J. Chen, and E. Baltsavias, Eds., Leiden, The Netherlands: CRC Press, 2008, pp. 157–167.

[2] P. A. Rosen *et al.*, "Synthetic aperture radar interferometry," *Proc. IEEE*, vol. 88, no. 3, pp. 333–382, Mar. 2000.

[3] M. Crosetto, B. Crippa, E. Biescas, O. Monseratt, M. Aguno, and P. Fernandez, "Land deformation monitoring using SAR interferometry: State-of-the-art," *Photogrammetrie, Fernerkundung, Geoinf.*, vol. 6, pp. 497–510, Jan. 2005.
[4] A. Ferretti, C. Prati, and F. Rocca, "Nonlinear subsidence rate estimation using permanent scatterers in differential SAR interferometry," *IEEE Trans. Geosci. Remote Sens.*, vol. 38, no. 5, pp. 2202–2012, Sep. 2000.
[5] A. Ferretti, C. Prati, and F. Rocca, "Permanent scatterers in SAR interferometry," *IEEE Trans. Geosci. Remote Sens.*, vol. 39, no 1, pp. 8–20, Jan. 2001.
[6] P. Berardino, G. Fornaro, R. Lanari, and E. Sansosti, "A new algorithm for surface deformation monitoring based on small baseline differential SAR interferograms," *IEEE Trans. Geosci. Remote Sens.*, vol. 40, no. 11, pp. 2375–2383, Nov. 2002.
[7] D. Arca, H. Ş. Kutoğlu, and K. Becek, "Landslide susceptibility mapping in an area of underground mining using the multicriteria decision analysis method," *Environ. Monit. Assessment*, vol. 190, no. 12, 2018, Art. no. 725.
[8] T. G. Farr *et al.*, "The shuttle radar topography mission," *Rev. Geophys.*, vol. 45, no. 2, May 2007, doi: 10.1029/2005RG000183.
[9] B. Rabus, M. Eineder, A. Roth, and R. Bamler, "The shuttle radar topography mission—A new class of digital elevation models acquired by spaceborne radar," *ISPRS J. Photogrammetry Remote Sens.*, vol. 57, no. 4, pp. 241–262, Apr. 2003.
[10] E. Rodriguez, C. S. Morris, and J. E. Belz, "A global assessment of the SRTM performance," *Photogrammetric Eng. Remote Sens.*, vol. 72, no. 3, pp. 249–260, Mar. 2006.
[11] K. Becek, "Investigating error structure of shuttle radar topography mission elevation data product," *Geophys. Res. Lett.*, vol. 35, no. 15, pp. L15403.1–L15403.5, Aug. 2008.
[12] K. Becek, "Assessing global digital elevation models using the runway method: The advanced spaceborne thermal emission and reflection radiometer versus the shuttle radar topography mission case," *IEEE Trans. Geosci. Remote Sens.*, vol. 52, no. 8, pp. 4823–4831, Aug. 2014.
[13] K. Becek, *Biomass Representation in Synthetic Aperture Radar Data Sets: A Comprehensive Study of Biomass-Induced Elevation Bias in DEMs Derived Using Synthetic Aperture Radar Interferometry*. Saarbrucken, Germany: LAP Lambert Academic Publishing, 2011.
[14] G. Krieger *et al.*, "TanDEM-X: A satellite formation for high-resolution SAR interferometry," *IEEE Trans. Geosci. Remote Sens.*, vol. 45, no. 11, pp. 3317–3341, Nov. 2007.
[15] K. Becek, W. Koppe, and Ş. H. Kutoğlu, "Evaluation of vertical accuracy of the WorldDEM^{TM} using the runway method," *Remote Sens.*, vol. 8, no. 11, Aug. 2016, Art. no. 938.
[16] ESA, "Sentinel online," 2020. [Online]. Available: https://sentinel.esa.int/web/sentinel/home
[17] A. Yilmaz and M. Erdoğan, "Designing high-resolution countrywide DEM for turkey," *Int. J. Eng. Geosci.*, vol. 3, no. 3, pp. 98–107, Oct. 2018.
[18] R. Lanari *et al.*, "An overview of the small baseline subset algorithm: A DInSAR technique for surface deformation analysis," *Pure Appl. Geophys.*, vol. 164, no. 4, pp. 637–661, Apr. 2007.
[19] F. Casu, M. Manzo, and R. Lanari, "Performance analysis of the SBAS algorithm for surface deformation retrieval," presented at the Fringe, Frascati, Italy, 2005.
[20] F. Casu, M. Manzo, and R. Lanari, "A quantitative assessment of the SBAS algorithm performance for surface deformation retrieval," *Remote Sens. Environ.*, vol. 102, no. 3–4, pp. 195–210, Jun. 2006.
[21] R. F. Hanssen, *Radar Interferometry*. Norwell, MA, USA: Kluwer, 2001.
[22] F. Amelung, D. L. Galloway, J. W. Bell, H. A. Zebker, and R. J. Laczniak, "Sensing the ups and downs of Las Vegas: InSAR reveals structural control of land subsidence and aquifer-system deformation," *Geology*, vol. 27, no. 6, pp. 483–486, Jun. 1999.
[23] R. Lanari, P. Lundgren, M. Manzo, and F. Casu, "Satellite radar interferometry time series analysis of surface deformation for Los Angeles, California," *Geophys. Res. Lett.*, vol. 31, no. 23, pp. L23613.1–L23613.5, 2004.
[24] J. C. L. Normand and E. Heggy, "InSAR assessment of surface deformations in urban coastal terrains associated with groundwater dynamics," *IEEE Trans. Geosci. Remote Sens.*, vol. 53, no. 12, pp. 6356–6371, Dec. 2015.
[25] C.-W. Lee, Z. Lu, H.-S. Jung, J.-S. Won, and D. Dzurisin, "Surface deformation of Augustine Volcano, 1992–2005, from multiple-interferogram processing using a refined small baseline subset (SBAS) interferometric synthetic aperture radar (InSAR) approach," in *The 2006 Eruption of Augustine Volcano, Alaska*, J. A. Power, M. L. Coombs, and J. T. Freymueller, Eds., U.S. Geological Survey, 2010, Ch. 18, no. 1769, pp. 453–465, 2010.
[26] K. Goel and N. Adam, "A distributed scatterer interferometry approach for precision monitoring of known surface deformation phenomena," *IEEE Trans. Geosci. Remote Sens.*, vol. 52, no. 9, pp. 5454–5468, Sep. 2014.
[27] D. R. Sandwell, X. Mellors, T. M. Wei, and P. Wessel, "Open radar interferometry software for mapping surface deformation," *Eos*, vol. 92, no. 28, pp. 234–235, Jul. 2011.
[28] C. W. Chen and H. A. Zebker, "Two-dimensional phase unwrapping with the use of statistical models for cost functions in nonlinear optimization," *J. Opt. Soc. Amer. A.*, vol. 18, no. 2, pp. 338–351, 2001.
[29] N. B. Avsar, S. Jin, Ş. H. Kutoğlu, and G. Gurbuz, "Vertical land motion along the black sea coast from satellite altimetry, tide gauges and GPS," *Adv. Space Res.*, vol. 60, no. 12, pp. 2871–2881, 2017.
[30] R. M. Norton, "The double exponential distribution: Using calculus to find a maximum likelihood estimator," *Amer. Statistician*, vol. 38, no. 2, pp. 135–136, May 1984.
[31] T. Tadono *et al.*, "Generation of the 30 m-mesh global digital surface model by ALOS PRISM," *Int. Arch. Photogrammetry Remote Sens. Spatial Inf. Sci.*, vol. XLI, no. B4, pp. 157–162, Jul. 2016.
[32] X. Li, H. Shen, R. Feng, J. Li, and L. Zhang, "DEM generation from contours and a low-resolution DEM," *ISPRS J. Photogrammetry Remote Sens.*, vol. 134, pp. 135–147, Dec. 2017.
[33] K. Becek, Ş. H. Kutoğlu, D. Glabicki, Ç. Bayık, J. Blachowski, and S. Abdikan, "Zonguldak, Turkey: Mining-induced land deformation in 2018–2019 - Sentinel 1 SBAS results," *Mendeley Data*, v1, Apr. 2020, doi: 10.17632/szhw6k2bsv.1

Kazimierz Becek (Senior Member, IEEE) received the Dipl.-Ing. (M.Sc.) degree in land surveying from the Wroclaw University of Agriculture, Wroclaw, Poland, in 1978, the Ph.D. degree in geodesy from the Dresden University of Technology, Dresden, Germany, in 1987, with a computer simulation thesis of atmospheric refraction, and the D.Sc. (Habilitation) degree in remote sensing from the Dresden University of Technology, Dresden, Germany, in 2010, with a thesis on biomass representation in InSAR datasets.

He is currently a Professor with the Wroclaw University of Environmental and Life Sciences, Wroclaw, Poland. He worked with the School of Surveying, UNSW, Sydney, Australia, from 1989 to 1994, before joining a publishing house on the Gold Coast, Australia, in 1995, as the Head of the Cartography and Data Acquisition Department. He also worked for the Queensland state government and the Gold Coast City local government (both in Australia) from 1998. From 2003 to 2013, he worked with the Geography Department, University of Brunei Darussalam, teaching Cartography, GIS, Photogrammetry, Remote Sensing, Geodesy, and Surveying. His research interests include mathematical modeling of environmental systems, including landslide monitoring, natural hazard mapping, and remote sensing methods for environmental studies.

Dr. Becek is a former Vice-President of the Brunei Institution of Geomatics.

Khairunnisa Ibrahim received the Bachelor of Arts degree in geography from University Brunei Darussalam, Gadong, Brunei, in 2006 and the M.Sc. degree in environmental informatics from the University of Leicester, Leicester, U.K., in 2009. She is currently working toward the D.Phil. degree in information, communication and the social sciences with the Oxford Internet Institute, University of Oxford, Oxford, U.K.

She joined University Brunei Darussalam after her masters, and from 2010 to 2013, she worked closely with Dr. K. Becek to teach modules and facilitate workshops on spatial information technologies and analyses for government and military officers. She was one of two Chevening Scholars awarded by the United Kingdom from Brunei Darussalam for 2008–2009. In addition, her master's thesis, on mapping the changes in proboscis monkey habitat along Sungai Brunei, Brunei Darussalam, was awarded the RICS East Region University Prize For Best Dissertation from Geographical Information Science and Environmental Informatics, University of Leicester, U.K. and the Royal Geographical Society's Planning and Environment Research Group (PERG) Masters Dissertation Prize.

Caglar Bayik was born in Hatay, Turkey, in 1986. He received the B.Sc., M.Sc., Ph.D. degrees in geomatics engineering from the Zonguldak Bülent Ecevit University, Zonguldak, Turkey, in 2010, 2012, and 2018, respectively.

Since 2011, he has been a Research Assistant with the Department of Geomatics Engineering, Zonguldak Bülent Ecevit University. In addition, he has experience in remote sensing and GIS applications. His research interests include SAR remote sensing, SAR Interferometry, deformation monitoring, and information extraction from SAR and optical images.

Saygin Abdikan received the B.S. degree in geodesy and photogrammetry engineering from Yildiz Technical University, Istanbul, Turkey, in 2004, and the M.Sc. and Ph.D. degrees in geomatics engineering, remote sensing and GIS program from Yildiz Technical University, in 2007 and 2013, respectively.

From 2005 to 2010, he was a Research Assistant with the Department of Geomatics Engineering, Yildiz Technical University. He was awarded Huygens Scholarship by Dutch Government and studied for two years from 2009 to 2011 in the radar group of Geoscience and Remote Sensing Department, Delft University of Technology, Delft, The Netherlands. Between 2014 and 2020, he worked with the Department of Geomatics, Zonguldak Bulent Ecevit University, Turkey. Since 2020, he has been an Academic Staff with the Department of Geomatics, Hacettepe University, Ankara, Turkey. His research interests include SAR remote sensing, SAR Interferometry, deformation monitoring, and information extraction from SAR and optical images.

Dr. Abdikan has been the Secretary of the International Society of Photogrammetry and Remote Sensing Commission III, Working Group III/2 on Microwave Remote Sensing since 2016.

Hakan S. Kutoglu was born in Zonguldak, Turkey, in 1970. He received the B.Sc., M.Sc., and Ph.D. degrees in geomatics engineering from the Istanbul Technical University, Istanbul, Turkey, in 1997, and 2001, respectively.

From 1994 to 2001, he was a Research Assistant with the Department of Geomatics Engineering, Zonguldak Bülent Ecevit University, Zonguldak, Turkey, where he was an Assistant Professor from 2001 to 2006, an Associate Professor from 2006 to 2012, and is currently a Professor. He developed the Figure Condition Method for Datum Transformation and Geometric Corrections of Satellite Images and carried out many types of research on the North Anatolian Fault's tectonics. Also, he carried out one of the first studies that applied Artificial Intelligence to solve geodetic problems. His research interests focus on geodetic coordinate systems, tectonic geodesy, and monitoring Earth changes.

Dariusz Glabicki was born in Kalisz, Poland, in 1994. He received the B.Sc. degree in geodesy and cartography and the M.Sc. degree in mining and geology (with a speciality in geoinformatics) in 2017 and 2018, respectively, from the Wrocław University of Science and Technology, Wrocław, Poland, where he is currently working toward the Ph.D. degree in mining and engineering geology.

His research interests include deformation mapping using the satellite radar interferometry techniques, mitigation of atmospheric disturbances in interferometry studies, applying machine learning in mining deformation analysis, and developing automatic systems for large area InSAR processing.

Jan Blachowski received the M.Sc. degree in mining and engineering geology and the Ph.D. degree in mining and geology from the Wroclaw University of Science and Technology, Wrocław, Poland, in 1999 and 2003, respectively.

He currently holds the position of Deputy Head of the Mining and Geodesy Department. In 2008, he was a Researcher with the Norwegian University of Science and Technology, Norway, and in 2012 with the University of New Brunswick, Canada. He is the author of 140 articles, conference papers, monographs and book chapters, and editor of conference proceedings. His research interests include analyzing and modeling natural and anthropogenic systems in geographic information systems, including mining-related terrain deformations with GIS.

Dr. Blachowski has been the recipient of two Polish National Science Centre research grants and is an active member of the Polish Association for Spatial Information, International Society for Mine Surveying, and International Society for Photogrammetry and Remote Sensing.